

# Low-Synch Gram-Schmidt with Delayed Reorthogonalization for Krylov Solvers

Daniel Bielich, Julien Langou, Stephen Thomas, Kasia Świrydowicz, Ichitaro Yamazaki, Erik G. Boman

## Abstract

The parallel strong-scaling of Krylov iterative methods is largely determined by the number of global reductions required at each iteration. The GMRES and Krylov-Schur algorithms compute the Arnoldi expansion for nonsymmetric matrices. The underlying algorithm is “left-looking” and processes one column at a time. Thus, at least one global reduction is required per iteration. The usual method for generating the orthogonal Krylov basis for the Krylov-Schur algorithm is classical Gram Schmidt applied twice (CGS2), requiring three global reductions per iteration. A new variant of CGS2 that requires only one reduction per iteration is applied to the Arnoldi-*QR* iteration. Strong-scaling results are presented for finding eigenvalue-pairs of nonsymmetric matrices. A preliminary attempt to derive a similar parallel method (one reduction per Arnoldi iteration with a robust orthogonalization scheme) was presented by Hernandez et al. [1]. Unlike our approach, their method is not forward stable for eigenvalues.

*Keywords:* Krylov methods, scalable, low synchronization

## 1. Introduction

The Rolling Stones [2] - You Can't Always Get What You  
Want ...

No, you can't always get what you want  
You can't always get what you want  
You can't always get what you want  
But if you try sometimes, well you just might find  
You get what you need

Let  $A$  be an  $n \times n$  real-valued matrix, where  $b$  and  $x$  are  $n \times 1$  vectors,  $m$  is a positive integer with  $m \ll n$ . In this manuscript,  $A$  appears in the context of two parallel distributed-memory computations: (1) finding a solution of the linear system  $Ax = b$  with a Krylov subspace method such as GMRES [3] and (2) finding the eigenvalues of  $A$  using Krylov-Schur [4]. In both instances, an orthogonal Krylov basis is required.

The Gram-Schmidt process produces a linearly independent basis. Krylov methods for linear system and eigenvalue solvers both depend upon the orthogonality of the basis for the Krylov subspace  $\mathcal{K}_m$  in finite precision arithmetic. The Arnoldi algorithm applies the Gram-Schmidt process to the Krylov basis which is the columns of  $Q_m$  in the factorization  $Q_m^T A Q_m = H_m$ . The loss of orthogonality of the computed basis – as measured by  $\|I - Q_m^T Q_m\|_F$  – may deviate substantially from machine precision  $O(\varepsilon)$ . When linear independence is completely lost, the Krylov iterations, may fail to converge. For the solution of linear systems of equations  $Ax = b$ , Paige et al. [5] show that when  $O(\varepsilon)\kappa(B)$ , for the Arnoldi matrix  $B = [r_0, A Q_m]$ , then MGS-GMRES is backward stable for the solution of linear systems. Here,  $\kappa(B)$  is the condition number  $\kappa(B) = \sigma_{\max}(B)/\sigma_{\min}(B)$ , where  $\sigma_i(B)$  are the singular values of a matrix  $B$ . For eigenvalue computations employing Krylov-Schur, accurate and converged eigenvalue approximations are obtained when the loss

of orthogonality remains close to  $O(\varepsilon)$ . In this paper, a stable Arnoldi algorithm is presented that performs well on a distributed-memory parallel computer.

Krylov linear system and eigenvalue solvers are often required for extreme scale physics simulations and implemented on parallel (distributed memory) machines. Their parallel strong-scaling is limited by the number and frequency of global reductions, in the form of MPI\_AllReduce. These communication patterns are expensive [6]. Our new algorithms are designed such that they require only one reduction to normalize each vector and apply projections. The focus here is on methods that process the Krylov vectors one column at a time as opposed to blocks (e.g. only one column becomes available at a time, and thus the vectors are processed in a “left-looking” fashion). As indicated previously, the Krylov basis size  $m$ , is assumed to be much smaller than the dimension  $n$  of the matrix  $A$ .  $Q_m$  is then referred to as a tall and skinny matrix. These are typical of Krylov iterative methods for solving a linear system of equations or eigenvalue problems, which rely on the Arnoldi expansion.

Classical Gram-Schmidt (CGS) is preferred for parallel computation because it requires only two global reductions for each column vector (a projection step, followed by a vector normalization). In practice, however, CGS leads to numerical instability for the solution of  $Ax = b$  and also eigenvalues, because the loss of orthogonality is  $O(\varepsilon)\kappa^2(A)$ . This bound was conjectured for a long time and finally proven in two papers [7, 8]. The GMRES iteration will stall and fail to converge if linear independence of the Krylov vectors is completely lost, for example, when  $\|S\|_2 = 1$  as described by Paige [9], where the matrix  $S$  was introduced in Paige et al. [5]. In order to obtain backward stable eigenvalues from Krylov-Schur, Stewart [4] demonstrates that  $O(\varepsilon)$  orthogonality suffices.

To reduce the loss of the orthogonality to machine precision  $O(\varepsilon)$ , the CGS algorithm can be applied twice (CGS2) to

reorthogonalize the basis vectors. This is the “twice is enough” result from Kahan and Parlett [10], which has also been proven by Giraud et. al. in [7]. Given the assumption that  $c\epsilon\kappa(A) < 1$  for a given  $m \times n$  input matrix  $A$  and constant  $c = O(m^2n^3)$ , then CGS2 can construct orthogonal columns to machine precision, Theorem 2 in [7]. The number of floating point operations (flops) for CGS2 is therefore  $4mn^2$  (twice the cost of CGS), and requires three global reductions.

A one-reduce variant of CGS2 was derived in [11] and is applied to the Arnoldi- $QR$  iteration in this paper. It achieves the same  $O(\epsilon)$  loss of orthogonality as the original CGS2 but requires only one reduction per column vector. To reduce the number of global reductions and avoid cancellation errors, the normalization step is lagged and the Pythagorean theorem is employed. The reorthogonalization is also delayed to the next iteration and thus is performed “on-the-fly” as opposed to a second pass. The resulting algorithm combines these two steps into one global reduction and is referred to as the delayed DCGS2 (this is explained in detail in Section 3.).

Extensive numerical results are presented for the Krylov-Schur eigenvalues to demonstrate the numerical stability and accuracy of DCGS2-Arnoldi. Strong-scaling results are presented for the ORNL Summit supercomputer to demonstrate that the DCGS2 algorithm improves the CGS2 execution times by a factor of up to  $2\times$  on GPUs, while maintaining the same loss of orthogonality as the original CGS2-Arnoldi algorithm.

## 2. Low-Synch Gram-Schmidt Algorithms

The development of low-synch MGS and CGS2 was largely driven by applications that need stable, yet scalable solvers. Even though MGS-GMRES is backward stable for the solution of linear systems, CGS2-GMRES was found to be more scalable for massively parallel computation in a 1998 study by Fraysé et al. [12] and included in the Trillinos framework by Bavier et al. [13]. The more recent development of a one-reduce MGS-GMRES by Swirydowicz et al. [11] implies that a re-evaluation of these results is certainly warranted in the context of a one-reduce DCGS2.

As already stated, the CGS2 algorithm requires three global reductions per iteration: one for the first projection, another for the second pass and a third for the normalization. The one-reduce DCGS2 delays reorthogonalization. This is achieved by lagging the normalization as originally proposed by Kim and Chronopoulos [14]) and then applying Stephen’s trick. The Pythagorean trick introduced by Smoktunowicz et al. [8] avoids cancellation errors and Carson et al. [15] generalize this to block Gram-Schmidt algorithms. The delayed normalization for the Arnoldi iteration was employed by Hernandez et al. [1] without a correction. DCGS2-Arnoldi as derived by these authors is not forward stable for eigenvalue computations because the loss of orthogonality is at least  $O(\epsilon)\kappa(B)$ , see Section 6. Delaying the normalization also requires a scaling to update the Krylov vectors in the Arnoldi expansion. Recent work [11, 16] describe a one-reduce inverse compact WY MGS algorithm with a triangular solve in the projection step. This ICWY-MGS requires only one reduction per iteration, the same as DCGS2. The

original modified Gram-Schmidt (MGS) requires  $2mn^2$  flops (the same as CGS) and applies the elementary rank-1 projections  $I - q_jq_j^T$  sequentially, requiring a separate global reduction for each inner-product. The complexity of ICWY-MGS is also  $2mn^2$ . The loss of orthogonality for MGS is  $O(\epsilon)\kappa(A)$  (see Björck in 1967 [17]). Whereas, it is  $O(\epsilon)$  for CGS2.

An MGS2, analogous to CGS2, exists. In practice, MGS2 exhibits an  $O(\epsilon)$  loss of orthogonality. The number of flops for MGS2 is  $4mn^2$ . (Double the cost of CGS or MGS and the same as CGS2). Low synch MGS2 requires  $4mn^2$  flops ( $2mn^2$  for the first pass and  $2mn^2$  for the second pass). These costs will be important considerations in strong scaling studies of these new algorithms on the ORNL Summit supercomputer.

## 3. DCGS2 Algorithm for the $QR$ Factorization

In this section, the classical Gram-Schmidt algorithm to compute the  $QR$  factorization is reviewed, where the matrix  $A$  has dimensions  $m \times n$ . Algorithm 1 displays the steps for the  $j$ -th iteration of CGS2. The column vector  $a_j$  is orthogonalized against the column vectors of  $Q_{1:j-1}$  using a single projection

$$\begin{aligned} w_j &= \left( I - Q_{1:j-1} Q_{1:j-1}^T \right) a_j \\ &= a_j - Q_{1:j-1} S_{1:j-1,j} \quad \text{where} \quad S_{1:j-1,j} = Q_{1:j-1}^T a_j, \end{aligned}$$

followed by a second application of the projector in the form

$$u_j = w_j - Q_{1:j-1} C_{1:j-1,j} \quad \text{where} \quad C_{1:j-1,j} = Q_{1:j-1}^T w_j.$$

Finally, the vector  $u_j$  is normalized to produce the vector  $q_j$ ,

$$q_j = u_j / \alpha_j \quad \text{where} \quad \alpha_j = \|u_j\|_2.$$

The  $QR$  factorization of  $A_{1:j} = Q_{1:j} R_{1:j,1:j}$ , is produced at the end of the  $j$ -th iteration, where

$$r_{1:j-1,j} = S_{1:j-1,j} + C_{1:j-1,j} \quad \text{and} \quad r_{j,j} = \alpha_j.$$

The three global reductions appear in steps 1, 3, and 5.

---

### Algorithm 1 Classical Gram-Schmidt (CGS2)

---

- ```

// first projection
1:   $S_{1:j-1,j} = Q_{1:j-1}^T a_j$  // global reduction
2:   $w_j = a_j - Q_{1:j-1} S_{1:j-1,j}$ 

// second projection
3:   $C_{1:j-1,j} = Q_{1:j-1}^T w_j$  // global reduction
4:   $u_j = w_j - Q_{1:j-1} C_{1:j-1,j}$ 

// normalization
5:   $\alpha_j = \|u_j\|_2$  // global reduction
6:   $q_j = u_j / \alpha_j$ 

// representation  $r_j$ 
7:   $r_{1:j-1,j} = S_{1:j-1,j} + C_{1:j-1,j}$ 
8:   $r_{j,j} = \alpha_j$ 

```
- 

The  $j$ -th iteration of DCGS2 is displayed in Algorithm 2. In order to obtain one global reduction, the second projection

and normalization are lagged or delayed to the next iteration. The purpose of the Pythagorean trick is to mitigate cancellation errors due to finite precision arithmetic. Namely, the norm of the updated vector  $u_j$  is computed as follows

$$\begin{aligned}\alpha_j^2 &= \left( w_j - Q_{1:j-1} C_{1:j-1,j} \right)^T \left( w_j - Q_{1:j-1} C_{1:j-1,j} \right) \\ &= w_j^T w_j - 2C_{1:j-1,j}^T C_{1:j-1,j} \\ &+ C_{1:j-1,j}^T \left( Q_{1:j-1}^T Q_{1:j-1} \right) C_{1:j-1,j} \\ &= w_j^T w_j - C_{1:j-1,j}^T C_{1:j-1,j}\end{aligned}$$

where  $C_{1:j-1,j} = Q_{1:j-1}^T w_j$  and the orthogonality of  $Q_{1:j-1}$  is assumed in finite precision arithmetic to be  $O(\varepsilon)$ . This corresponds to Step 3 in Algorithm 2.

Because the normalization is delayed, Stephen's trick allows us to compute the norm with  $w_{j-1}$  versus  $u_{j-1}$  at the beginning of each iteration. Finally, for the column vector  $a_j$ , the scalar  $S_{j-1,j}$  is computed by using  $S_{j-1,j} = w_{j-1}^T a_j$  instead of  $q_{j-1}^T a_j$ . Therefore, after the computation of  $w_{j-1}$ , the norm must be corrected.

$$\begin{aligned}q_{j-1}^T a_j &= \frac{1}{\alpha_{j-1}} \left( w_{j-1} - Q_{1:j-2} C_{1:j-2,j-1} \right)^T a_j \\ &= \frac{1}{\alpha_{j-1}} \left( w_{j-1}^T a_j - C_{1:j-2,j-1}^T Q_{1:j-2}^T a_j \right) \\ &= \frac{1}{\alpha_{j-1}} \left( S_{j-1,j} - C_{1:j-2,j-1}^T S_{1:j-2,j} \right)\end{aligned}$$

This correction corresponds to step 7 (Stephen's trick) in Algorithm 2 given below. For the final  $n$ -th iteration, CGS2 is

---

**Algorithm 2** Delayed Classical Gram-Schmidt (DCGS2)

---

- 1: Compute  $[Q_{1:j-2}, w_{j-1}]^T [w_{j-1}, a_j]$ 

$$S_{1:j-2,j} = Q_{1:j-2}^T a_j \quad \text{and} \quad S_{j-1,j} = w_{j-1}^T a_j$$

$$C_{1:j-2,j-1} = Q_{1:j-2}^T w_{j-1} \quad \text{and} \quad \beta_{j-1} = w_{j-1}^T w_{j-1}$$
  - 2:  $u_{j-1} = w_{j-1} - Q_{1:j-2} C_{1:j-2,j-1}$ 

*// delayed reorthogonalization*
  - 3:  $\alpha_{j-1} = \left\{ \beta_{j-1} - C_{1:j-2,j-1}^T C_{1:j-2,j-1} \right\}^{1/2}$ 

*// delayed normalization*
  - 4:  $q_{j-1} = \frac{1}{\alpha_{j-1}} u_{j-1}$ 

*// projection*
  - 5:  $S_{j-1,j} = \frac{1}{\alpha_{j-1}} \left( S_{j-1,j} - C_{1:j-2,j-1}^T S_{1:j-2,j} \right)$
  - 6:  $w_j = a_j - Q_{1:j-1} S_{1:j-1,j}$ 

*// representation  $r_{j-1}$*
  - 7:  $r_{1:j-2,j-1} = S_{1:j-2,j-1} + C_{1:j-2,j-1}$
  - 8:  $r_{1:j-2,j} = S_{1:j-2,j}$
  - 9:  $r_{j-1,j-1} = \alpha_{j-1}$
- 

applied. This incurs two additional global reductions.

#### 4. DCGS2 Algorithm for the Arnoldi Expansion

Algorithm 3 displays CGS2 for the Arnoldi expansion. The only difference from the  $QR$  factorization in Algorithm 1 is that the next basis vector  $v_j$  is generated by applying the sparse-matrix vector multiply (SpMV) to the previously normalized column vector  $q_{j-1}$ . At the end of iteration  $j-1$ , in exact arithmetic, the matrices would satisfy the Arnoldi expansion,

$$A Q_{1:j-2} = Q_{1:j-1} H_{1:j-1,j-2}. \quad (1)$$

---

**Algorithm 3** Arnoldi- $QR$  (CGS2)

---

- 1:  $v_j = A q_{j-1}$ 

*// generation of next vector*
  - 2:  $T_{1:j-1,j} = Q_{1:j-1}^T v_j$
  - 3:  $w_j = v_j - Q_{1:j-1} T_{1:j-1,j}$ 

*// first projection*
  - 4:  $C_{1:j-1,j} = Q_{1:j-1}^T w_j$
  - 5:  $u_j = w_j - Q_{1:j-1} C_{1:j-1,j}$ 

*// second projection*
  - 6:  $\alpha_j = \|u_j\|_2$
  - 7:  $q_j = \frac{1}{\alpha_j} u_j$ 

*// normalization*
  - 8:  $H_{1:j-1,j} = T_{1:j-1,j} + C_{1:j-1,j}$
  - 9:  $H_{j,j} = \alpha_j$ 

*// representation  $H_j$*
- 

The one-reduction DCGS2-Arnoldi will now be derived. The representation error and loss of orthogonality are maintained at the same level as the CGS2-Arnoldi.

With lagged vector updates, the next basis vector is generated by applying an SpMV to the current vector. Namely, the next vector  $v_j$  is computed as  $A w_{j-1}$  by using the vector  $w_{j-1}$  instead of  $q_{j-1}$ , where  $q_{j-1}$  is the resulting vector. Thus, an effective strategy is required to compute  $w_j$  from  $A w_{j-1}$  and also to generate the Hessenberg matrix  $H_j$  in the Arnoldi expansion.

After a delay of one iteration, the vector  $q_{j-1}$ , is computed using  $w_{j-1}$  as follows

$$q_{j-1} = \frac{1}{\alpha_{j-1}} \left( w_{j-1} - Q_{1:j-2} C_{1:j-2,j-1} \right) \quad (2)$$

Equation (2) may also be interpreted as a  $QR$  factorization of the matrix  $W_{1:j-1}$ , with columns  $[w_1, \dots, w_{j-1}]$

$$Q_{1:j-1} = W_{1:j-1} C_{1:j-1,1:j-1}^{-1}, \quad (3)$$

where  $C$  is an upper triangular matrix.

Multiplying (2) by  $A$  from the left, it follows that

$$\begin{aligned}v_j &= A q_{j-1} \\ &= \frac{1}{\alpha_{j-1}} \left( A w_{j-1} - A Q_{1:j-2} C_{1:j-2,j-1} \right) \\ &= \frac{1}{\alpha_{j-1}} \left( A w_{j-1} - Q_{1:j-1} H_{1:j-1,1:j-2} C_{1:j-2,j-1} \right)\end{aligned} \quad (4)$$

Next the vector  $w_j$  is computed, which is the vector produced after orthogonalizing  $v_j$  against the basis vectors in  $\mathcal{Q}_{1:j-1}$ ,

$$\begin{aligned} w_j &= A q_{j-1} - \mathcal{Q}_{1:j-1} \mathcal{Q}_{1:j-1}^T A q_{j-1} \\ &= \frac{1}{\alpha_{j-1}} \left( A w_{j-1} - \mathcal{Q}_{1:j-1} H_{1:j-1,1:j-2} C_{1:j-2,j-1} \right. \\ &\quad \left. - \mathcal{Q}_{1:j-1} \mathcal{Q}_{1:j-1}^T \right) \\ &\times \frac{1}{\alpha_{j-1}} \left( A w_{j-1} - \mathcal{Q}_{1:j-1} H_{1:j-1,1:j-2} C_{1:j-2,j-1} \right) \\ w_j &= \frac{1}{\alpha_{j-1}} \left( A w_{j-1} - \mathcal{Q}_{1:j-1} \mathcal{Q}_{1:j-1}^T A w_{j-1} \right) \\ &+ \frac{1}{\alpha_{j-1}} \mathcal{Q}_{1:j-1} \left( I - \mathcal{Q}_{1:j-1}^T \mathcal{Q}_{1:j-1} \right) H_{1:j-1,1:j-2} C_{1:j-2,j-1} \end{aligned} \quad (5)$$

The last term is dropped from (5), for two reasons,

- DCGS2 is constructed such that the loss of orthogonality  $\|I - \mathcal{Q}_{1:j-1}^T \mathcal{Q}_{1:j-1}\|_F$  is  $\mathcal{O}(\varepsilon)$ , and
- $C_{1:j-2,j-1}/\alpha_{j-1}$  is expected to be  $\mathcal{O}(\varepsilon)\kappa(A)$ . Hence, when  $\kappa(A) \leq \mathcal{O}(1/\varepsilon)$ , the norm of the term is  $\mathcal{O}(1)$ .

Therefore, at this point the = sign is now an approximation and

$$\begin{aligned} w_j &= \frac{1}{\alpha_{j-1}} \left( A w_{j-1} - \mathcal{Q}_{1:j-1} \mathcal{Q}_{1:j-1}^T A w_{j-1} \right) \\ &= \frac{1}{\alpha_{j-1}} \left( A w_{j-1} - \mathcal{Q}_{1:j-2} \mathcal{Q}_{1:j-2}^T A w_{j-1} \right) \\ &\quad - \frac{1}{\alpha_{j-1}} q_{j-1} q_{j-1}^T A w_{j-1} \end{aligned}$$

Noting that  $S_{1:j-2,j} = \mathcal{Q}_{1:j-2}^T A w_{j-1}$ , it follows that

$$w_j = \frac{1}{\alpha_{j-1}} \left( A w_{j-1} - \mathcal{Q}_{1:j-2} S_{1:j-2,j} - q_{j-1} q_{j-1}^T A w_{j-1} \right)$$

Finally, from (2), it is possible to compute

$$\begin{aligned} q_{j-1}^T A w_{j-1} &= \frac{1}{\alpha_{j-1}} \left( w_{j-1} - \mathcal{Q}_{1:j-2} C_{1:j-2,j-1} \right)^T A w_{j-1} \\ &= \frac{1}{\alpha_{j-1}} \left( w_{j-1}^T A w_{j-1} - C_{1:j-2,j-1}^T \mathcal{Q}_{1:j-2}^T A w_{j-1} \right) \\ &= \frac{1}{\alpha_{j-1}} \left( S_{j-1,j} - C_{1:j-2,j-1}^T S_{1:j-2,j} \right) \end{aligned}$$

where  $S_{j-1,j} = w_{j-1}^T A w_{j-1}$ . This step is Stephen's trick in the context of Arnoldi.

After substitution of this expression, it follows that

$$\begin{aligned} w_j &= \frac{1}{\alpha_{j-1}} \left( A w_{j-1} - \mathcal{Q}_{1:j-2} S_{1:j-2,j} \right) \\ &\quad - \frac{1}{\alpha_{j-1}^2} q_{j-1} \left( S_{j-1,j} - C_{1:j-2,j-1}^T S_{1:j-2,j} \right) \\ &= \frac{1}{\alpha_{j-1}} A w_{j-1} - \mathcal{Q}_{1:j-1} T_{1:j-1,j} \end{aligned} \quad (6)$$

where

$$T_{1:j-2,j} = \frac{1}{\alpha_{j-1}} S_{1:j-2,j}$$

and

$$T_{j-1,j} = \frac{1}{\alpha_{j-1}^2} \left( S_{j-1,j} - C_{1:j-2,j-1}^T S_{1:j-2,j} \right).$$

The  $(j-1)$ -th column of the Hessenberg matrix  $H$  is computed as follows and satisfies the Arnoldi relation (1). First, reorder (6) into a factorization form

$$\begin{aligned} A w_{j-1} &= \mathcal{Q}_{1:j-2} S_{1:j-2,j} \\ &\quad + \frac{1}{\alpha_{j-1}} q_{j-1} \left( S_{j-1,j} - C_{1:j-2,j-1}^T S_{1:j-2,j} \right) + \alpha_{j-1} w_j \end{aligned} \quad (7)$$

From (2), it also follows that

$$w_j = \mathcal{Q}_{1:j-1} C_{1:j-1,j} + \alpha_j q_j \quad (8)$$

which represents the orthogonalization of the vector  $w_j$ . By replacing  $w_j$  in (7) with the expression in (8), obtain

$$\begin{aligned} A w_{j-1} &= \mathcal{Q}_{1:j-2} S_{1:j-2,j} \\ &\quad + \frac{1}{\alpha_{j-1}} q_{j-1} \left( S_{j-1,j} - C_{1:j-2,j-1}^T S_{1:j-2,j} \right) \\ &\quad + \alpha_{j-1} \mathcal{Q}_{1:j-1} C_{1:j-1,j} + \alpha_j \alpha_{j-1} q_j \\ A w_{j-1} &= \mathcal{Q}_{1:j-2} \left( S_{1:j-2,j} + \alpha_{j-1} C_{1:j-2,j} \right) \\ &\quad + \frac{1}{\alpha_{j-1}} q_{j-1} \left( S_{j-1,j} - C_{1:j-2,j-1}^T S_{1:j-2,j} \right) \\ &\quad + \alpha_{j-1} C_{j-1,j} q_{j-1} + \alpha_j \alpha_{j-1} q_j. \end{aligned} \quad (9)$$

This is the representation of  $A w_{j-1}$  in the Krylov subspace having orthogonal basis vectors  $\mathcal{Q}_{1:j}$  using the matrices  $S$  and  $C$ . However, the representation of  $A q_{j-1}$  in  $\mathcal{Q}_{1:j}$  is needed with the matrix  $H$ . Namely, write (5) as

$$\begin{aligned} A q_{j-1} &= \frac{1}{\alpha_{j-1}} \left( A w_{j-1} - \mathcal{Q}_{1:j-2} H_{1:j-2,1:j-2} C_{1:j-2,j-1} \right) \\ &\quad - \frac{1}{\alpha_{j-1}} q_{j-1} H_{j-1,j-2} C_{j-2,j-1} \end{aligned}$$

$H_{j-1,j-1}$  is now computed using  $C_{j-2}$  and  $H_{1:j-1,j-2}$ .

Replacing  $A w_{j-1}$  with (9), it follows that

$$\begin{aligned} A q_{j-1} &= \mathcal{Q}_{1:j-2} \left( \frac{1}{\alpha_{j-1}} S_{1:j-2,j} + C_{1:j-2,j} \right) \\ &\quad + \frac{1}{\alpha_{j-1}^2} q_{j-1} \left( S_{j-1,j} - C_{1:j-2,j-1}^T S_{1:j-2,j} \right) \\ &\quad + \alpha_j q_j - \frac{1}{\alpha_{j-1}} \mathcal{Q}_{1:j-2} H_{1:j-2,1:j-2} C_{1:j-2,j-1} \\ &\quad + C_{j-1,j} q_{j-1} - \frac{1}{\alpha_{j-1}} H_{j-1,j-2} C_{j-2,j-1} q_{j-1} \end{aligned} \quad (10)$$

To summarize

1.  $A q_{j-1} = \mathcal{Q}_{1:j-2} A_{1:j-2,j} + q_{j-1} s_{j-1,j} + \alpha_j q_j$  is a standard  $QR$  factorization obtained by a Gram-Schmidt process.
2.  $C_{1:j-2,j}$  and  $C_{j-1,j}$  are the reorthogonalization terms in the representation equation,
3.  $C_{1:j-2,j-1}^T S_{1:j-2,j}$  is Stephen's trick.
4.  $H_{1:j-2,1:j-2} C_{1:j-2,j-1}$  and  $H_{j-1,j-2} C_{j-2,j-1}$  are the representation error correction terms.

Items 1, 2 and 3 are present in both the  $QR$  and Arnoldi factorizations. Items 4 and 5 are specific to Arnoldi.

According to (10), in order to satisfy the  $(j-1)$ -th column of the Arnoldi relation (1), the column  $H_{1:j,j-1}$  is computed as follows

$$\begin{aligned} H_{1:j-2,j-1} &= \frac{1}{\alpha_{j-1}} S_{1:j-2,j} + C_{1:j-2,j} \\ &- \frac{1}{\alpha_{j-1}} H_{1:j-2,1:j-2} C_{1:j-2,j-1} \\ &= T_{1:j-2,j} + C_{1:j-2,j} - \frac{1}{\alpha_{j-1}} H_{1:j-2,1:j-2} C_{1:j-2,j-1} \end{aligned}$$

where  $H_{j-1,j-2} = \alpha_{j-1}$ , and

$$\begin{aligned} H_{j-1,j-1} &= \frac{1}{\alpha_{j-1}^2} \left( S_{j-1,j} - C_{1:j-2,j-1}^T S_{1:j-2,j} \right) + C_{j-1,j} \\ &- \frac{1}{\alpha_{j-1}} H_{j-1,j-2} C_{j-2,j-1} \\ H_{j,j-1} &= \alpha_j \end{aligned}$$

Finally, the DCGS2–Arnoldi is presented in Algorithm 4.

---

**Algorithm 4** Arnoldi- $QR$  (DCGS2)

---

- 1: Compute  $[Q_{1:j-2}, w_{j-1}]^T [w_{j-1}, Aw_{j-1}]$
  - 2:  $S_{1:j-2,j} = Q_{1:j-2}^T Aw_{j-1}$  and  $S_{j-1,j} = w_{j-1}^T Aw_{j-1}$
  - 3:  $C_{1:j-2,j-1} = Q_{1:j-2}^T w_{j-1}$  and  $\beta_{j-1} = w_{j-1}^T w_{j-1}$
  - // delayed normalization*
  - 4:  $\alpha_{j-1} = \left\{ \beta_{j-1} - C_{1:j-2,j-1}^T C_{1:j-2,j-1} \right\}^{1/2}$
  - 5:  $T_{j-1,j} = \frac{1}{\alpha_{j-1}^2} \left( S_{j-1,j} - C_{1:j-2,j-1}^T S_{1:j-2,j} \right)$
  - 6:  $T_{1:j-2,j} = \frac{1}{\alpha_{j-1}} S_{1:j-2,j}$
  - // projection*
  - 7:  $u_{j-1} = w_{j-1} - Q_{1:j-2} C_{1:j-2,j-1}$
  - 8:  $q_{j-1} = \frac{1}{\alpha_{j-1}} u_{j-1}$
  - 9:  $w_j = \frac{1}{\alpha_{j-1}} Aw_{j-1} - Q_{1:j-1} T_{1:j-1,j}$
  - // representation  $H_{j-1}$*
  - 10:  $H_{1:j-2,j-2} = K_{1:j-2,j-2} + C_{1:j-2,j-1}$
  - 11:  $K_{1:j-1,j-1} = T_{1:j-1,j} - \frac{1}{\alpha_{j-1}} H_{1:j-1,1:j-2} C_{1:j-2,j-1}$
  - 12:  $H_{j-1,j-2} = \alpha_{j-1}$
- 

## 5. Computation and Communication Costs

The computation and communication costs of the algorithms are listed in Tables 1 and 2. Although theoretically equivalent, they exhibit different behaviour in finite precision arithmetic. All the schemes, except MGS, are based upon cache-blocked matrix operations. MGS applies elementary rank-1 projection matrices sequentially to a vector and does not take advantage of the DGEMM matrix-matrix multiplication kernel. In addition,

this algorithm requires one global reduction (MPI\_AllReduce) in the inner loop to orthogonalize a vector, i.e.,  $j+1$  global reductions at the  $j$ -th iteration. The implementation of ICWY-MGS batches together the projections and computes one row of the strictly lower triangular matrix [11].

$$L_{k-1,1:k-2} = \left( Q_{1:k-2}^T q_{k-1} \right)^T.$$

The resulting inverse compact  $WY$  projector  $P$  is given by

$$P a = \left( I - Q_{j-1} T_{j-1} Q_{j-1}^T \right) a$$

where the triangular correction matrix is given by

$$T_{j-1} = (I + L_{j-1})^{-1}, \quad T_{j-1} \approx (Q_{j-1}^T Q_{j-1})^{-1}$$

The implied triangular solve requires an additional  $j^2$  flops at the  $j$ -th iteration and leads to the slightly higher operation count compared to the original MGS. However, only one global reduction is required, and hence the amount of parallel communication does not depend upon the number of vectors to be processed.

In the case of the DCGS2 algorithm, the correction matrix was derived in Appendix 1 of [11] and is given by

$$T_{j-1} = I - L_{j-1} - L_{j-1}^T.$$

This form of the projector was employed in the  $s$ -step GMRES described in [16]. When the matrix  $T_{j-1}$  is split into  $I - L_{j-1}$  and  $L_{j-1}^T$  and applied across two iterations of the DCGS2 algorithm, the resulting loss of orthogonality is  $O(\varepsilon)$  in practice.

| orth scheme        | flops per iter   | synchs | bandwidth |
|--------------------|------------------|--------|-----------|
| MGS                | $4(m/p)j$        | $j$    | $j$       |
| MGS ICWY           | $6(m/p)j + 2j^2$ | 1      | $2j$      |
| CGS                | $4(m/p)j$        | 2      | $j$       |
| CGS2               | $8(m/p)j$        | 3      | $2j$      |
| CGS2 (lagged norm) | $8(m/p)j$        | 2      | $2j$      |
| DCGS2              | $8(m/p)j + j^2$  | 1      | $2j$      |

Table 1: Cost per iteration for Gram Schmidt algorithms

| orth scheme        | flops per iter               | synchs           | bandwidth        |
|--------------------|------------------------------|------------------|------------------|
| MGS                | $2(m/p)n^2$                  | $\frac{1}{2}n^2$ | $\frac{1}{2}n^2$ |
| MGS ICWY           | $3(m/p)n^2$                  | $n$              | $n^2$            |
| CGS                | $2(m/p)n^2$                  | $2n$             | $\frac{1}{2}n^2$ |
| CGS2               | $4(m/p)n^2$                  | $3n$             | $n^2$            |
| CGS2 (lagged norm) | $4(m/p)n^2$                  | $2n$             | $n^2$            |
| DCGS2              | $4(m/p)n^2 + \frac{1}{3}n^3$ | $n$              | $n^2$            |

Table 2: Total cost of Gram Schmidt algorithms

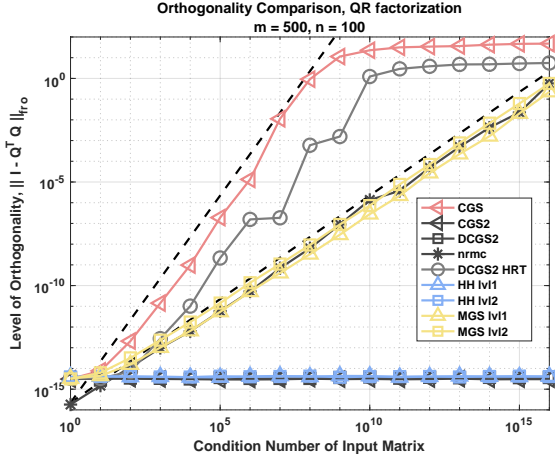


Figure 1: Loss of orthogonality with increasing condition number.

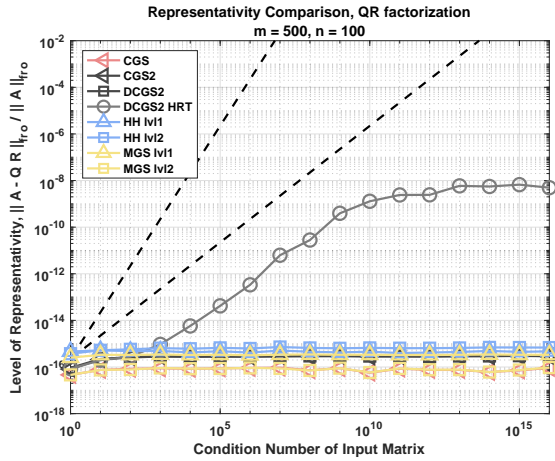


Figure 2: Representation error with increasing condition numbers.

Both CGS and CGS2 are based upon matrix-vector operations. CGS applies a single projection, and then normalizes, requiring two separate steps. This projection step consists of two DGEMV kernel calls and one DDOT for the normalization. CGS suffers from at least an  $O(\epsilon)\kappa^2(A)$  loss of orthogonality. CGS2 achieves  $O(\epsilon)$  through two passes (see Figure 1). The additional projection within CGS2 accounts for one additional global reduction per iteration and an additional  $4(m/p)j$  operations.

DCGS2 requires one reduction and employs matrix-matrix multiplies for the computation in a tall-and-skinny DGEMM. This leads to the higher sustained execution rate of DCGS2 compared with CGS2 (e.g.  $2\times$  the GigaFlop/sec). In the context of Arnoldi, DCGS2 requires an additional  $j^2$  flops at the  $j$ -th iteration. The additional cost is due to the Arnoldi representation trick explained in Section 4. The correction term requires an additional  $n^2$  operations from a matrix-vector product with the Hessenberg matrix.

| orth scheme        | LOO                      | Proven      |
|--------------------|--------------------------|-------------|
| MGS                | $O(\epsilon)\kappa(A)$   | [17]        |
| MGS ICWY           | $O(\epsilon)\kappa(A)$   | Conjectured |
| CGS                | $O(\epsilon)\kappa^2(A)$ | [7]         |
| CGS2               | $O(\epsilon)$            | [7]         |
| CGS2 (lagged norm) | $O(\epsilon)$            | Conjectured |
| DCGS2              | $O(\epsilon)$            | Conjectured |

Table 3: Loss of Orthogonality (LOO).

## 6. Numerical Results

In this section, the numerical properties of the Arnoldi iteration are determined experimentally as formal proofs of backward stability are forthcoming

### 6.1. Manteuffel Matrix

The matrix generated by “central differences” presented by Manteuffel [18] is employed in tests of the Krylov-Schur eigenvalue solver based upon DCGS2–Arnoldi. The matrix is convenient for computing the forward error. The Manteuffel matrix is expressed as the sum

$$A = \frac{1}{h^2}M + \frac{\beta}{2h}N \quad (11)$$

where the matrix blocks and eigenvalues are generated by

$$\lambda_{i,j} = 2 \left[ 2 - \sqrt{1 - \left(\frac{\beta}{2}\right)^2 \left( \cos\left(\frac{i\pi}{L}\right) + \cos\left(\frac{j\pi}{L}\right) \right)} \right]. \quad (12)$$

$L$  is defined by the domain of the differential operator,  $[0, L] \times [0, L]$  and  $h = L / (n + 1)$ . The matrix scales to any size and an explicit formula exists for the eigenvalues. For the experiments,  $\beta = 0.5$  and  $L = n + 1$  so that  $h = 1$  ( $\beta \leq 2$  implies all eigenvalues are real).  $M$  and  $N$  are  $n \times n$  block diagonal matrices,  $M$  is positive definite and  $N$  is skew-symmetric. For  $n = 50$ , relevant numerical metrics are summarized in Table 4. Here,  $V$  and  $W$  are the left and right eigenvectors. The Manteuffel matrix is employed to evaluate the convergence of Krylov-Schur.

|                                   |           |
|-----------------------------------|-----------|
| $\ A\ _2$                         | 7.9925+00 |
| $\text{Cond}(A)$                  | 3.3184+02 |
| $\text{Cond}(V)$                  | 3.9560+11 |
| $\text{Cond}(W)$                  | 3.7415+11 |
| $\ A^T A - A A^T\ _F / \ A\ _F^2$ | 2.8053-04 |
| $\max(\text{Cond}(\lambda_i, j))$ | 1.4579+10 |
| $\min(\text{Cond}(\lambda_i, j))$ | 2.3777+02 |

Table 4: Differential operator specs for  $n = 50$ ,  $m = n^2 = 2500$ .

The Arnoldi residual and error metrics employed herein are described in Hernández et al/ [19]. Figure 3 displays the loss of orthogonality  $\|I_j - Q_j^T Q_j\|_F$ , while Figure 4 is a plot of the Arnoldi relative representation error, from equation (1)

$$RRE = \frac{\|A Q_{j-2} - Q_{j-1} H_{j-1, j-2}\|_F}{\|A\|_F}.$$

Each of the algorithms, except for the DCGS2-HRT presented in [1], achieve machine precision level relative error. Figure 4 displays the loss of orthogonality for each scheme. It was noted earlier that CGS exhibits an  $O(\varepsilon)\kappa^2(A)$  loss of orthogonality. The plot illustrates that DCGS2-HRT follows CGS while the other algorithms construct orthonormal columns to the level of machine precision.

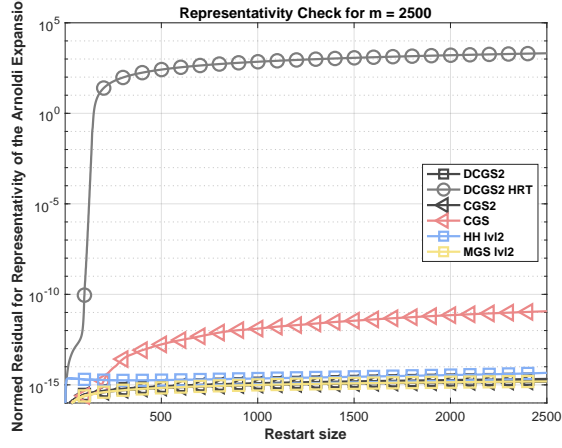


Figure 3: Loss of orthogonality.

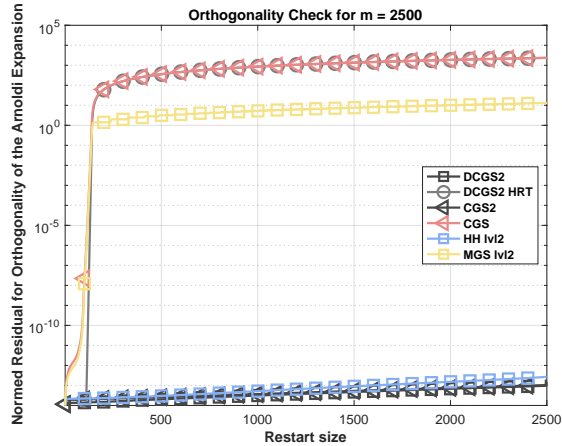


Figure 4: Representation error.

The results from a Krylov-Schur eigenvalue experiment to evaluate the convergence properties of the different Arnoldi iterations are plotted in Figure 5. The solver relies upon the Schur decomposition of the Hessenberg matrix  $H_m$  generated in the Arnoldi expansion. To assess the convergence rates, the Arnoldi residual [1] is compared to the absolute error tolerance. The approximate eigenvector (or Ritz vector) associated with the eigenvalue  $\lambda_i$  is defined by  $z_i = V_m y_i$ , where  $y_i$  is the corresponding eigenvector of  $H_m$ .

$$\|(A - \lambda_i I) z_i\|_2 = h_{m+1,m} |e_m^T y_i| < \text{tol}$$

where  $\text{tol} = 1e-7$ . If this threshold is satisfied, the Arnoldi iteration is considered to have found an invariant subspace and the associated diagonal element in the Schur triangular matrix

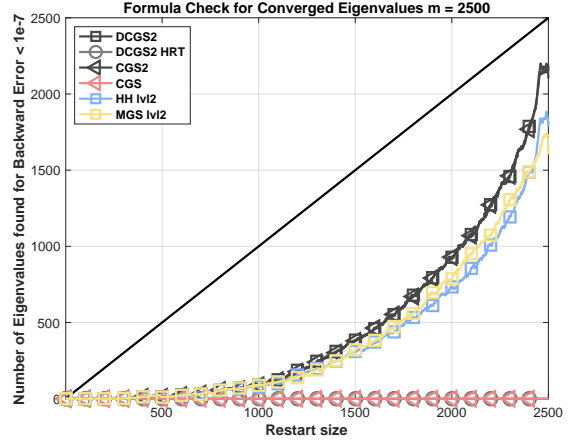


Figure 5: Number of eigenvalues computed with  $1e-7$  absolute error.

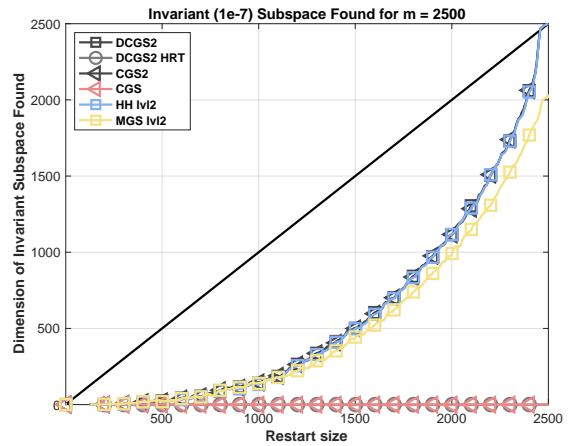


Figure 6: Number of invariant subspaces computed.

$T$  is an eigenvalue. The benefit of using the Manteuffel matrix is that exact analytic expressions for the eigenvalues are available and thus the representation error and loss of orthogonality can be easily computed. If these quantities are not close to machine precision, a converged invariant subspace has not been found. After the size of the invariant subspace has been determined, the  $n^2$  eigenvalues from the formula in 12 are computed and compared with the “converged” eigenvalues in the Schur triangular matrix  $T$ . In addition, rather than computing the same eigenvalue twice, the multiplicity is determined. This is a check to determine if the Krylov-Schur algorithm continually re-computes the same eigenvalue, or unique eigenvalues through this decomposition. The exact multiplicity of any given eigenvalue was always found.

The left plot in Figure 5 displays the converged eigenvalues according to  $|\lambda_{i,j} - T_{k,k}| < \text{tol}$ , where  $\text{tol} = 1e-7$ . The solid line indicates that if a perfect Arnoldi expansion were available, with a Krylov subspace dimension (restart) of  $m = 50$ , then it is possible to produce 50 converged eigenvalues. Figure 6 displays the size of the invariant subspaces found. None of the methods can follow this line, but as the full Arnoldi expansion of the Manteuffel matrix is approached, any scheme that maintains orthogonality can continually find new eigenvalues. Com-

paring both plots illustrates that in practice, when eigenvalues are not known, looking at the size of the invariant subspaces can be a good metric. Note that between the two plots, there is a small gap for the error formula at a restart of 2500, where this gap is not present in the invariant subspace plot. The different Arnoldi variants cannot find all of the invariant subspaces, which is due to the condition number of the eigenvalues. Comparing the different  $QR$  factorization schemes and the invariant subspaces found, although it loses orthogonality, Arnoldi with MGS can still find new search directions. Arnoldi- $QR$  based on Householder (HH), CGS2 and DCGS2, can find a subspace that spans the entire space, but for this matrix MGS still performs well and generates a subspace size close to 2000.

## 6.2. Matrix Market

The Arnoldi- $QR$  factorization algorithms are now compared for matrices gathered from the SuiteSparse collection maintained by Tim Davis at Texas A&M University [20]. A total of 635 matrices were chosen by the following criteria: (1) number of nonzeros  $< 500,000$ , (2) the matrix is REAL, (3) the matrix is UNSYMMETRIC and (4) the number of columns and rows  $> 100$ . With this collection, the Krylov basis is computed for each of the 635 matrices. The representation error and loss of orthogonality are computed for every 5 columns until 75 (making sure the dimension of any matrix is not exceeded). Meaning the restart in an Arnoldi expansion varies from 5 to 75 in increments of 5.

Figures 7 and 8 display these metrics for each of the schemes. At each iteration the tolerance is set to  $1e-7$ . If the representation error or loss of orthogonality is above this threshold the matrix is flagged. The y-axis represents the total number of matrices above the given threshold and the x-axis indicates the Krylov subspace dimension (restart) employed by the Arnoldi expansion.

Figure 8 clearly indicates that Krylov vectors generated using CGS and MGS lose orthogonality at different rates. It is observed that the DCGS2-HRT curve falls between these. For the Manteuffel matrix, DCGS2-HRT appears to perform more like CGS and lies somewhere in between. It is important to note, in Figure 7, that DCGS2-HRT does not maintain a low representation error for the Arnoldi expansion. This is also apparent in Figure 2.

With an Arnoldi restart of  $k = 75$ , these metrics are plotted in Table 5. The additional metric displayed is the size of the invariant subspace found, described in Section 6.1.

| Orth. scheme | Repres $< 1e-7$ | LOO $< 1e-7$ | Invariant Subspace |
|--------------|-----------------|--------------|--------------------|
| CGS          | <b>635</b>      | 374          | 8370               |
| DCGS2 HRT    | 435             | 463          | 7168               |
| CGS2         | <b>635</b>      | 622          | 9677               |
| DCGS2        | 631             | 621          | <b>9844</b>        |
| HH lvl2      | <b>635</b>      | <b>635</b>   | 9783               |

Table 5:  $k = 75$ ;  $tol = 1e-7$ ; SuiteSparse matrices

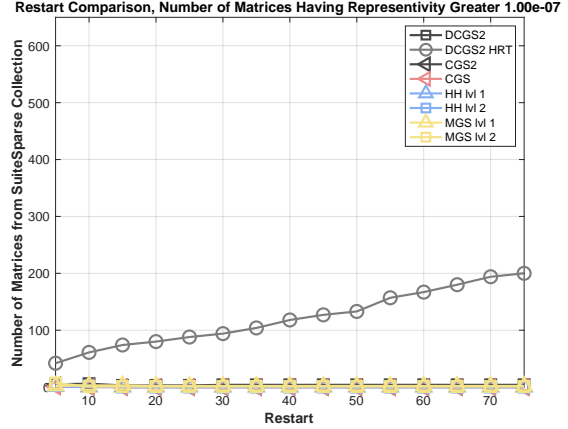


Figure 7: Representation error for SuiteSparse matrices.

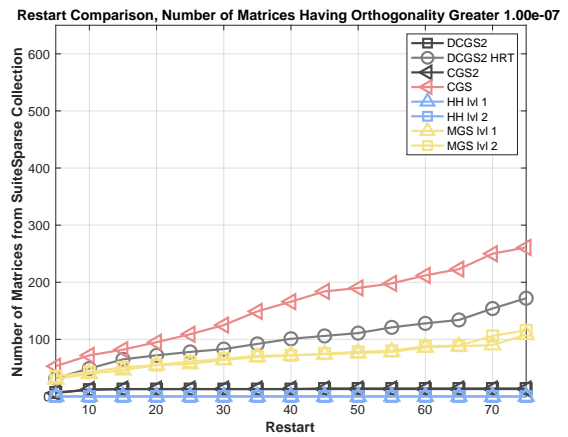


Figure 8: Loss of Orthogonality for SuiteSparse matrices.

## 7. Parallel Performance Results

Parallel performance results are now presented for the Summit Supercomputer at Oak Ridge National Laboratory. Each node of summit consists of two 22-core IBM Power 9 sockets and six NVIDIA Volta 100 GPUs. CGS2 and DCGS2 were implemented and tested using the Trilinos-Belos iterative solver framework [13, 21]. Therefore, although NVIDIA V100 GPU results are presented here, the implementation is portable to different hybrid node architectures with a single code base.

To summarize, DCGS2 achieves faster execution times than CGS2 for two reasons. First, the former employs either matrix-vector or matrix-matrix kernels, which provide greater potential for data reuse. For tall-and-skinny matrices, employed by DGEMV and DGEMM, compute time is often limited by data movement, and matrix-matrix type kernels often achieve faster execution rates. Therefore, DCGS2 is faster than CGS2, even on a single GPU. Second, on multiple GPUs, the low-synch algorithm decreases the number of global-reductions. Therefore, a greater speedup is achieved on a large number of GPUs. In this section, the execution rates on a single and multiple GPUs are compared.



### 7.1. Single GPU Performance

Figure 11 provides the execution rates in GigaFlops/sec of the main computational kernels on a single GPU, with an increasing number of rows or columns, respectively. In the plot,

- `MvTransMv` computes the dot-products, e.g., DGEMV to compute  $t_{1:j-1,j} = Q_{1:j-1}^T a_j$  in CGS2 or DGEMM to compute  $[Q_{1:j-2}, w_{j-1}]^T [w_{j-1}, a_j]$  in DCGS2.
- `MvTimesMatAddMv` updates the vectors by applying the projection, e.g., DGEMV to compute  $w_j = q_j - Q_{1:j-1} t_{1:j-1,j}$  in CGS2 or DGEMM to compute

$$[u_{j-1}, w_j] = [w_{j-1}, a_j] - Q_{1:j-2} [c_{1:j-2,j-1}, t_{1:j-2,j}]$$

- `MvDot` computes DDOT product of two vectors, and is used to compute the normalization factor  $c_{j,j} = \|u_j\|_2$ .

Figure 12 displays the time to solution, where both algorithms require  $4mn^2$  flops. It is observed that DCGS2 achieves a speedup of up to  $3.6\times$  faster compute times.

Memory bandwidth utilization is a predictor of performance. For example, at the  $j$ -th iteration of CGS2, `MvTransMv` reads the  $m \times (j-1)$  matrix  $Q_{1:j-1}$  and the input vector  $a_j$  of length  $m$ , then writes the result back to the output vector  $t_{1:j-1,j}$ , while performing  $(2m-1) \times (j-1)$  flops with two flops per read, assuming the vectors remain in caches, or two flops per two reads and one write with a read-write of vector elements for each multiply-add. Thus, on the V100 GPU with a memory bandwidth of 800 GB/s, 200 GigaFlops/sec is expected from this kernel in double precision. Figures 12a and 12a display kernel execution times on 30 Summit nodes as the number of rows or columns is varied.

Note that DCGS2 combines two `MvTransMv` calls with a single input and output vector into a single call to `MvTransMv` with two input and output vectors. This doubles the potential peak speed (i.e. the  $m \times (j-1)$  matrix is read only once to perform four flops per read). Figures 12a and 12a, indicate that for a large number of rows or columns, that DCGS2 lowers the execution time by up to  $2.2\times$ .

### 7.2. Parallel Strong-Scaling Performance

The speedups obtained by DCGS2 for the two main kernels are presented in Tables 6 and 7, while Figure 13 displays the GigaFlops/sec execution rate achieved by the kernels,

- Table 6 displays the speedup (ratio of DCGS2 to CGS2 compute time) for `MvTransMv`. Because DCGS2 employs fewer global reductions, as the number of GPUs increases, the speedup obtained by `MvTransMv` increases, reaching up to  $2.20\times$  faster times on 32 GPUs.
- Table 7 displays the speedup for the `MvTimesMatAddMv` kernel. DCGS2 merges two `MvTimesMatAddMv` calls into one `MvTimesMatAddMv` and achieves  $2\times$  speedup on a single GPU. With more GPUs, the number of local rows and speedup decrease. However, the compute time is dominated by the `MvTimesMatAddMv` kernel.

| # GPUs | Number of rows, $m$ |                |                 |                 |                 |
|--------|---------------------|----------------|-----------------|-----------------|-----------------|
|        | $1 \cdot 10^6$      | $5 \cdot 10^6$ | $10 \cdot 10^6$ | $25 \cdot 10^6$ | $50 \cdot 10^6$ |
| 6      | 1.7438              | 1.5704         | 1.5529          | 1.3101          | 1.1202          |
| 12     | 1.9129              | 1.7546         | 1.6661          | 1.5151          | 1.3218          |
| 24     | 2.0522              | 1.7344         | 1.7085          | 1.5728          | 1.5265          |
| 48     | 2.1295              | 1.8638         | 1.9172          | 1.7510          | 1.6158          |
| 96     | 1.9512              | 2.1162         | 4.0421          | 1.8204          | 1.7470          |
| 192.   | 2.1574              | 2.0830         | 2.2825          | 2.1000          | 2.2014          |

Table 6: Speedup obtained by DCGS2 for `MvTransMv` and `MvDot`.

| # GPUs | Number of rows, $m$ |                |                 |                 |                 |
|--------|---------------------|----------------|-----------------|-----------------|-----------------|
|        | $1 \cdot 10^6$      | $5 \cdot 10^6$ | $10 \cdot 10^6$ | $25 \cdot 10^6$ | $50 \cdot 10^6$ |
| 6      | 0.8387.             | 2.0058         | 2.0093          | 1.9600          | 1.9490          |
| 12     | 1.8759              | 1.9924         | 1.9408          | 1.9568          | 1.9409          |
| 24     | 1.2770              | 0.8891         | 1.1941          | 1.9802          | 1.9512          |
| 48     | 1.0463              | 0.8691         | 0.9185          | 1.9296          | 2.0043          |
| 96     | 1.0956              | 0.8012         | 5.1914          | 1.1147          | 1.3115          |
| 192.   | 0.8514              | 0.7419         | 0.6978          | 0.9421          | 1.2632          |

Table 7: Speedups obtained by DCGS2 for `MvTimesMatAddMv`.

Finally, Table 8 displays the speedup obtained by DCGS2, when varying the number of rows, and Figure 14 reports the total computation time. DCGS2 obtains a greater speedup as the number of GPUs increases.

Figure 13 displays the GigaFlops/sec execution rates obtained by CGS2 and DCGS2, along with the BLAS kernels for a fixed matrix size ( $m = 25 \cdot 10^6$  and  $n = 50$ ). The `MvTransMv` operation requires a global reduce, while the DGEMM operations do not require communication. DCGS2 always outperforms CGS2 in these runs. `MvTimesMatAddMv` perform similarly for both schemes on 96 and 192 nodes. CGS2 exhibits an increase in speed that matches DCGS2. For a large number of rows or columns, DCGS2 obtains about 66 GigaFlops/sec per node at 192 nodes or about 6% of the single GPU sustained execution rate of 200 GigaFlops/sec.

## 8. Conclusion

For parallel distributed-memory computation, two-passes of classical Gram-Schmidt (CGS2) was the method of choice

| # GPUs | Number of rows, $m$ |                |                 |                 |                 |
|--------|---------------------|----------------|-----------------|-----------------|-----------------|
|        | $1 \cdot 10^6$      | $5 \cdot 10^6$ | $10 \cdot 10^6$ | $25 \cdot 10^6$ | $50 \cdot 10^6$ |
| 6      | 1.0751              | 1.6216         | 1.6484          | 1.4998          | 1.3374          |
| 12     | 1.1235              | 1.7628         | 1.7236          | 1.6250          | 1.4985          |
| 24     | 1.0874              | 1.5049         | 1.7558          | 1.6620          | 1.6350          |
| 48     | 1.1516              | 1.1385         | 1.8051          | 1.7548          | 1.6844          |
| 96     | 1.2064              | 1.3210         | <b>3.5982</b>   | 1.7928          | 1.7692          |
| 192    | 1.4211              | 1.3095         | 1.7070          | 1.9015          | <b>2.1151</b>   |

Table 8: Overall speedups obtained by DCGS2.

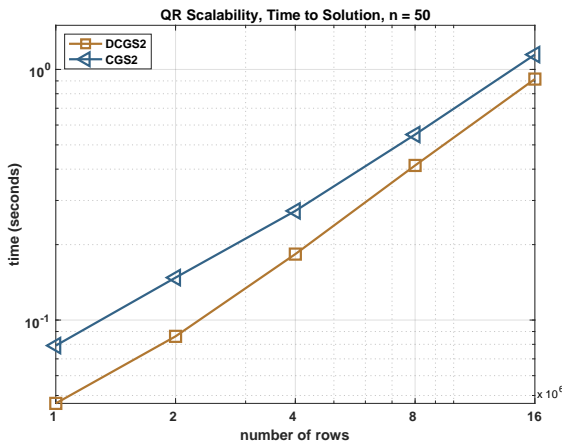
| Orthog Scheme | Number of rows, $m$ , in millions |       |       |       |       |
|---------------|-----------------------------------|-------|-------|-------|-------|
|               | 1                                 | 2     | 4     | 8     | 16    |
| DCGS2         |                                   |       |       |       |       |
| MVTimes GF/s  | 300.3                             | 319.1 | 302.3 | 320.3 | 331.4 |
| MVTrans GF/s  | 201.4                             | 211.8 | 191.4 | 150.2 | 126.8 |
| Total sec     | 215.1                             | 232.3 | 218.2 | 193.3 | 174.8 |
| CGS2          |                                   |       |       |       |       |
| MVTimes GF/s  | 132.0                             | 136.4 | 153.4 | 163.8 | 169.5 |
| MVTrans GF/s  | 128.5                             | 141.0 | 146.4 | 135.3 | 122.2 |
| Total sec     | 126.4                             | 135.4 | 146.7 | 145.5 | 139.6 |

(a) Fixed number of columns  $n = 50$ . GigaFlops/sec and time (sec)

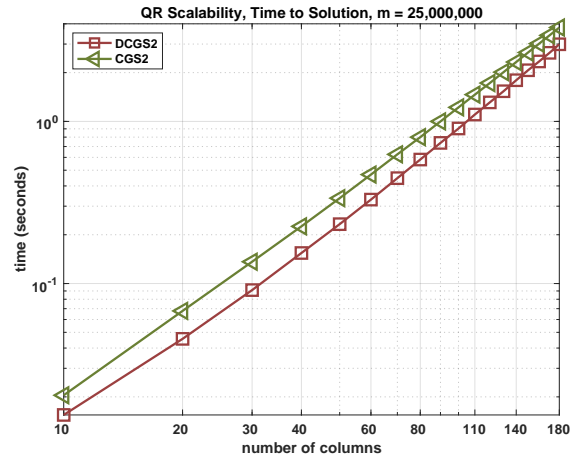
| Orthog Scheme | Number of columns, $n$ |       |       |       |       |
|---------------|------------------------|-------|-------|-------|-------|
|               | 100                    | 120   | 140   | 160   | 180   |
| DCGS2         |                        |       |       |       |       |
| MVTimes GF/s  | 353.7                  | 362.8 | 369.8 | 375.6 | 379.7 |
| MVTrans GF/s  | 169.2                  | 164.3 | 160.3 | 158.7 | 155.6 |
| Total sec     | 221.2                  | 219.8 | 218.4 | 218.5 | 216.6 |
| CGS2          |                        |       |       |       |       |
| MVTimes GF/s  | 182.1                  | 186.9 | 190.7 | 193.1 | 195.7 |
| MVTrans GF/s  | 152.0                  | 153.6 | 153.4 | 153.3 | 153.2 |
| Total sec     | 163.8                  | 167.1 | 168.6 | 169.7 | 170.8 |

(b) Fixed number of rows  $m = 5 * 10^6$ . GigaFlops/sec and time (sec)

Figure 9: Execution rate (GigaFlops/sec) of BLAS kernels (1 node of Summit).



(a) With varying number of rows.



(b) With varying numbers of columns.

Figure 10: Total orthogonalization time (1 node of Summit).

for Krylov solvers requiring machine precision level representation errors and loss of orthogonality. However, the algorithm requires three global reductions for each column of the  $QR$  factorization computed and thus the strong-scaling behaviour can deviate substantially from linear as the number of MPI ranks increases on Exascale class supercomputers such as the ORNL Summit. In this paper, a new variant of CGS2 that requires only one global reduction per iteration was applied to the Arnoldi- $QR$  algorithm. Our numerical results have demonstrated that DCGS2 obtains the same loss of orthogonality and representation error as CGS2, while our strong-scaling results on the Summit supercomputer indicate that DCGS2 obtains a speedup of  $2\times$  faster compute time on a single GPU, and an even larger speedup on an increasing number of GPUs, reaching  $2.2\times$  lower execution times on 192 GPUs. The impact of DCGS2 on the strong scaling of Krylov linear system solvers is currently being explored, and a block variant is also being implemented following the review article of Carson et al. [15]. The software employed for this paper is available on GitHub.

## Acknowledgement

Funding was provided by the Exascale Computing Project (17-SC-20-SC). The National Renewable Energy Laboratory is operated by Alliance for Sustainable Energy, LLC, for the U.S.

Department of Energy (DOE) under Contract No. DE-AC36-08GO28308. Sandia National Laboratories is a multimission laboratory managed and operated by National Technology & Engineering Solutions of Sandia, LLC, a wholly owned subsidiary of Honeywell International Inc., for the U.S. Department of Energy National Nuclear Security Administration under contract DE-NA0003525.

A portion of this research used resources of the Oak Ridge Leadership Computing Facility, that is a DOE Office of Science User Facility supported under Contract DE-AC05-00OR22725 and using computational resources sponsored by the Department of Energy's Office of Energy Efficiency and Renewable Energy and located at the National Renewable Energy Laboratory.

Julien Langou was supported by NSF award #1645514.

## References

- [1] V. Hernández, J. Román, A. Tomas, Parallel arnoldi eigensolvers with enhanced scalability via global communications rearrangement, *Parallel Computing* 33 (2007) 521–540. doi:10.1016/j.parco.2007.04.004.
- [2] T. R. Stones, *Let it bleed* (1969).
- [3] Y. Saad, M. H. Schultz, GMRES: A generalized minimal residual algorithm for solving nonsymmetric linear systems, *SIAM Journal on scientific and statistical computing* 7 (3) (1986) 856–869.

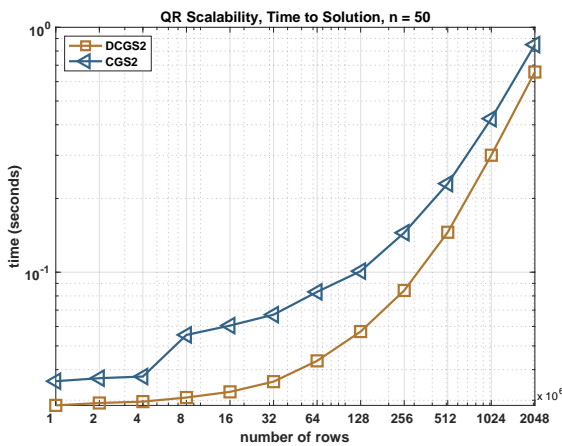
| Orthog Scheme | Number of rows, $m$ , in millions |       |       |       |       |
|---------------|-----------------------------------|-------|-------|-------|-------|
|               | 128                               | 256   | 512   | 1024  | 2048  |
| DCGS2         |                                   |       |       |       |       |
| MVTimes GF/s  | 194.2                             | 248.9 | 285.9 | 312.5 | 324.2 |
| MVTrans GF/s  | 129.4                             | 170.4 | 179.9 | 154.1 | 128.6 |
| Total sec     | 124.3                             | 168.9 | 195.4 | 189.4 | 173.2 |
| CGS2          |                                   |       |       |       |       |
| MVTimes GF/s  | 99.6                              | 126.6 | 145.1 | 158.9 | 167.1 |
| MVTrans GF/s  | 73.9                              | 100.8 | 124.9 | 128.4 | 119.3 |
| Total sec     | 42.8                              | 98.2  | 123.7 | 134.3 | 133.9 |

(a) Fixed number of columns  $n = 50$ . GigaFlops/sec and time (sec)

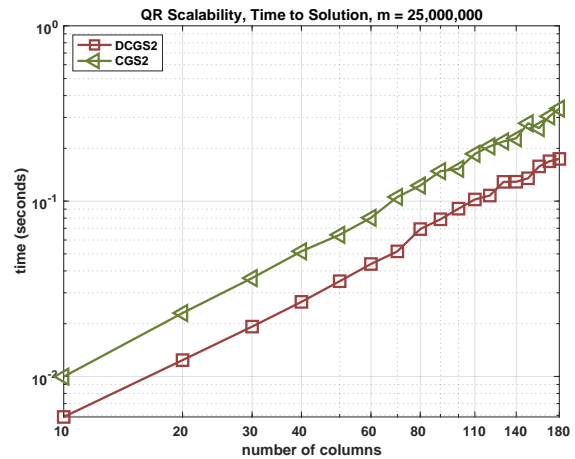
| Orthog Scheme | Number of columns, $n$ |       |       |       |       |
|---------------|------------------------|-------|-------|-------|-------|
|               | 100                    | 120   | 140   | 160   | 180   |
| DCGS2         |                        |       |       |       |       |
| MVTimes GF/s  | 121.6                  | 135.5 | 151.2 | 159.7 | 168.9 |
| MVTrans GF/s  | 61.1                   | 76.9  | 89.1  | 89.1  | 107.6 |
| Total sec     | 61.4                   | 74.4  | 84.4  | 90.1  | 103.4 |
| CGS2          |                        |       |       |       |       |
| MVTimes GF/s  | 122.2                  | 95.2  | 101.3 | 99.3  | 90.4  |
| MVTrans GF/s  | 38.1                   | 39.4  | 49.6  | 56.5  | 52.6  |
| Total sec     | 36.4                   | 38.9  | 47.7  | 54.5  | 53.4  |

(b) Fixed number of rows  $m = 25 * 10^6$ . GigaFlops/sec and time (sec)

Figure 11: Execution rate (GigaFlops/sec) of BLAS kernels (30 nodes of Summit).



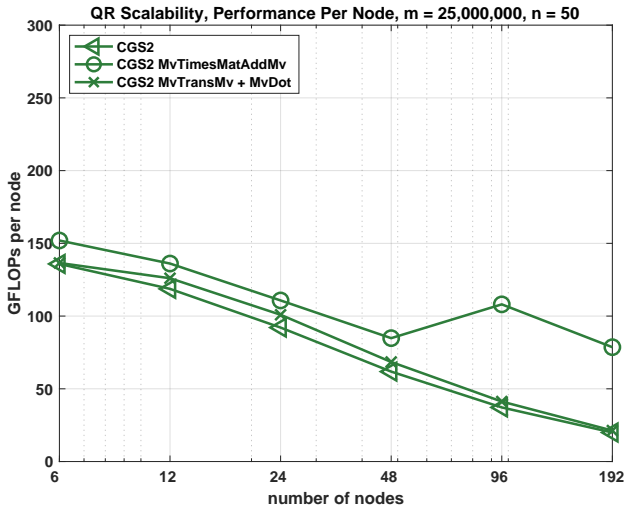
(a) With varying number of rows.



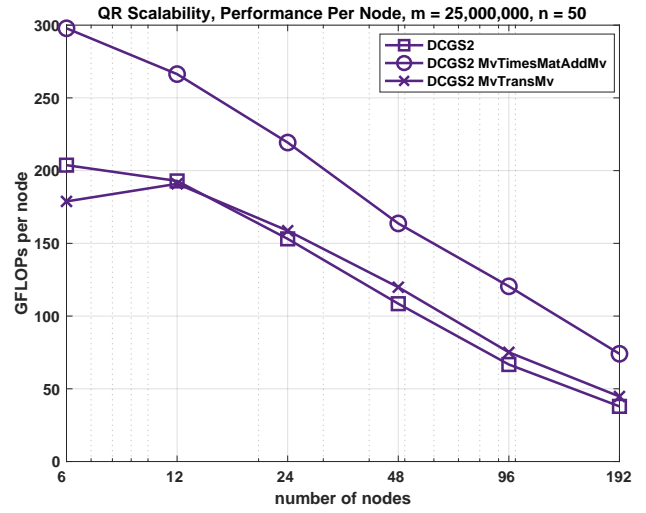
(b) With varying numbers of columns.

Figure 12: Total orthogonalization time (30 nodes of Summit).

- [4] G. W. Stewart, A Krylov–Schur algorithm for large eigenproblems, *SIAM Journal on Matrix Analysis and Applications* 23 (3) (2001) 601–614.
- [5] C. C. Paige, M. Rozložník, Z. Strakoš, Modified Gram–Schmidt (MGS), least squares, and backward stability of MGS–GMRES, *SIAM Journal on Matrix Analysis and Applications* 28 (1) (2006) 264–284. doi:10.1137/050630416.
- [6] A. Bienz, W. Gropp, L. Olson, Node-aware improvements to allreduce, in: *Proceedings of the 2019 IEEE/ACM Workshop on Exascale MPI (ExaMPI)*, Association for Computing Machinery, 2019.
- [7] L. Giraud, J. Langou, M. Rozložník, J. van den Eshof, Rounding error analysis of the classical Gram–Schmidt orthogonalization process, *Numerische Mathematik* 101 (1) (2005) 87–100. doi:doi:10.1007/s00211-005-0615-4.
- [8] A. Smoktunowicz, J. L. Barlow, J. Langou, A note on the error analysis of classical Gram–Schmidt, *Numerische Mathematik* 105 (2) (2006) 299–313. doi:doi:10.1007/s00211-006-0042-1.
- [9] C. Paige, The Effects of Loss of Orthogonality on Large Scale Numerical Computations, 2018, pp. 429–439. doi:10.1007/978-3-319-95168-3\_29.
- [10] B. N. Parlett, *The Symmetric Eigenvalue Problem*, Society for Industrial and Applied Mathematics, 1998. arXiv:https://epubs.siam.org/doi/pdf/10.1137/1.9781611971163, doi:10.1137/1.9781611971163. URL https://epubs.siam.org/doi/abs/10.1137/1.9781611971163
- [11] K. Świrydowicz, J. Langou, S. Ananthan, U. Yang, S. Thomas, Low synchronization Gram–Schmidt and generalized minimal residual algorithms, *Numerical Linear Algebra with Applications* (2020) 1–20doi:10.1016/j.jocs.2016.04.008.
- [12] V. Frayssé, L. Giraud, H. K. Aroussi, On the influence of the orthogonalization scheme on the parallel performance of GMRES, *Tech. Rep. TR-PA-98-07*, CERFACS (1998).
- [13] E. Bavier, M. Hoemmen, S. Rajamanickam, H. Thornquist, Amesos2 and Belos: Direct and iterative solvers for large sparse linear systems, *Scientific Programming* 20 (3) (2012) 241–255.
- [14] S. K. Kim, A. T. Chronopoulos, An efficient parallel algorithm for extreme eigenvalues of sparse nonsymmetric matrices, *International Journal of Supercomputer Applications* 6 (1) (1992) 98–111.
- [15] E. Carson, K. Lund, M. Rozložník, S. Thomas, An overview of block Gram–Schmidt methods and their stability properties (2020). arXiv:2010.12058.
- [16] I. Yamazaki, S. Thomas, M. Hoemmen, E. G. Boman, K. Świrydowicz, J. J. Elliott, Low-synchronization orthogonalization schemes for  $s$ -step and pipelined Krylov solvers in Trilinos, *SIAM*, 2020, pp. 118–128. URL https://epubs.siam.org/doi/abs/10.1137/1.9781611976137.11
- [17] A. Björck, Solving least squares problems by Gram–Schmidt orthogonalization, *BIT* 7 (1967) 1–21. doi:10.1007/BF01934122.
- [18] T. A. Manteuffel, Adaptive procedure for estimating parameters for the nonsymmetric Tchebychev iteration, *Numerische Mathematik* 31 (2) (1978) 183–208.
- [19] V. Hernández, J. Román, A. Tomas, V. Vidal, Krylov–Schur methods in SLEPc, *Tech. Rep. SLEPc Technical Report STR-7*, University of Valencia (2007).
- [20] T. A. Davis, Y. Hu, The university of florida sparse matrix collection, *ACM Trans. Math. Softw.* 38 (1) (Dec. 2011). doi:10.1145/2049662.2049663. URL https://doi.org/10.1145/2049662.2049663
- [21] M. Heroux, et. al., An overview of the Trilinos project, *ACM Trans. Math. Softw.* (2005).



(a) CGS2 execution rate on Summit.



(b) DCGS2 execution rate (GigaFlops/sec) on Summit.

Figure 13: CGS2 and DCGS2 strong-scaling.

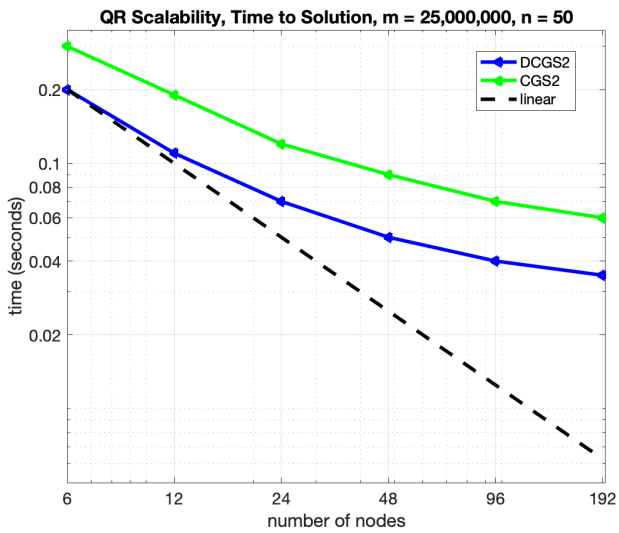


Figure 14: Time to solution on Summit.